Supporting Information for: Sustainable materials for renewable energy storage in the Thermal Battery

Samantha L. Piper,[a] Craig M. Forsyth,[a] Mega Kar,[b] Callum Gassner, [a] R. Vijayaraghavan,[c] S. Mahadevan,[c] Karolina Matuszek,*[a] Jennifer M. Pringle,[b] and Douglas R. MacFarlane *[a]

[a]*School of Chemistry, Monash University, Clayton, Victoria 3800, Australia*

[b]*Institute for Frontier Materials, Deakin University, Burwood Campus, Burwood, Victoria 3125, Australia*

[c]*Cell for Industrial Safety and Risk Analysis, CLRI, 6000-20 Chennai, India*

Emails: karolina.matuszek@monash.edu, douglas.macfarlane@monash.edu

Table of Contents

List of Figures and Tables

1. Materials and methods

Synthesis of C18-hx, C18-MDP, C18-cyhx, C18-Ph and C18-MePh

For all compounds, the respective diisocyanate was mixed at a 1:2 molar ratio with octadecanol in anhydrous THF. 5 mol% (relative to the moles of the diisocyanate) of 1,4-diazabicyclo[2.2.2]octane was added and the mixtures were heated with stirring at 60 °C for 2 days. For C18-hx, C18-MDP, C18-Ph and C18-cyhx, the subsequent solid was filtered and recrystallised in hot THF. For C18-MePh, the solution was concentrated by rotary evaporation and the resulting solid was recrystallised with hot ethanol.

C18-hx

Yield: 85%.**^{1}H NMR** (400 MHz, *$CDCl_3$*) δ 4.62 (s, 2H), 4.03 (t, 4H), 3.16 (m, 4H), 1.59 (m, 4H), 1.49 (m, 4H), 1.35-1.22 (m, 60H), 0.88 (t. 6H). **m/z =** 709.6875 $[M+H]^+$

C18-cyhx

Yield: 52%.**^{1}H NMR** (400 MHz, *$CDCl_3$*) δ 4.46 (s, 2H), 4.02 (t, 4H), 3.44 (m, 2H), 2.03 (d, 4H), 1.58 (m, 4H), 1.31-1.15 (m, 60H), 0.88 (t, 6H). **m/z =** 707.2, $[M+H]^+$.

C18-MDP

Yield: 82%.**^{1}H NMR** (400 MHz, *d_8-THF*) δ 8.53 (s, 2H), 7.36 (d, 2H), 7.03 (d, 2H), 4.07 (t, 4H), 3.83 (s, 2H), 1.64 (m, 4H), 1.24 (m, 60H), 0.90 (t, 6H). **m/z =** 791.6652, $[M+H]^+$.

C18-Ph

Yield: 88%.**^{1}H NMR** (400 MHz, *d_8-THF*) δ 8.48 (s, 2H), 7.35 (s, 4H), 4.06 (t, 4H), 1.63 (m, 4H), 1.28 (m, 59H), 0.88 (t, 6H). **m/z =** 701.6170, $[M+H]^+$.

C18-MePh

Yield: 79%.**^{1}H NMR** (400 MHz, *d_8-THF*) δ 8.63 (s, 1H), 7.77 (s, 1H), 7.66 (d, 1H), 7.37 (d, 1H), 7.01 (d, 1H), 4.11 (m, 4H), 2.20 (s, 3H), 1.69 (m, 4H), 1.33 (m, 60H), 0.93 (t, 6H). **m/z =** 715.6357, $[M+H]^+$.

Solvent-free synthesis of C18-hx

0.610 g (3.6 mmol) 1,6-hexamethylene diisocyanate was placed in a 25 mL two-necked RBF under a nitrogen flow. 1.965 g octadecanol (7.2 mmol) was added to the flask and the mixture was stirred at 90 °C. After ~ 5 minutes the mixture began to thicken and after 10 minutes the temperature was increased to 130 °C and the reaction was stirred for a further 50 minutes. Upon cooling, the resulting solid was analysed by DSC (ΔH_f = 202 J g^{-1}, T_m = 116 °C).**^{1}H NMR** (400 MHz, *d_8*-THF) δ 6.27 (s, 2H), 4.08 (t, 4H), 3.18 (m, 4H), 1.69 (m, 4H), 1.59 (m, 4H), 1.50-1.35 (m, 60H), 1.03 (t, 6H).

Synthesis of C16-hx-C18

0.1236 g (0.735 mmol) 1,6-hexamethylene diisocyanate, 0.1782 g (0.735 mmol) hexadecanol and 0.1988 g octadecanol (0.735 mmol) were placed in a small Monowave 50 reactor tube with 5 mL THF. In the monowave reactor, the mixture was heated at 125 °C for one hour. The resulting solid was filtered and washed with THF. Yield: 81%. DSC: ΔH_f = 178 J g^{-1}, T_m = 113 °C. **^{1}H NMR** (400 MHz, *d_8*-THF) δ 6.26 (s, 1H), 5.46 (s, 1H), 4.08 (t, 4H), 3.20 (m, 4H), 1.70 (m, 4H), 1.57 (m, 4H), 1.52-1.31 (m, 58H), 1.03 (t, 6H).

2. Characterisation

Differential scanning calorimetry (DSC)

Transition temperatures (T_m, T_{s-s}) and enthalpies of fusion were determined using a DSC Perkin-Elmer differential scanning calorimeter with a heating rate of 10 °C/min except when stated otherwise. Sample sizes for these measurements were within a mass range of 4 – 10

mg, and samples were hermetically sealed in aluminium pans for the analysis. The DSC was calibrated with indium (T_m = 156.6 °C, ΔH_f = 28.45 J/g and cyclohexane (T_m = 8 °C) standards. Measurements were performed under a nitrogen atmosphere with an N_2 flow rate of 50 mL/min. Each sample was cycled three times, and thermal data is reported from the second heating and cooling cycles. ΔH_f was calculated according to the integration under the endothermic transition peak, using Pyris software.

While researchers, including ourselves, often define T_m as the peak temperature of a melting transition, this clearly represents an upper bound on the true melting point because of thermal lag in the instrument and the sample. However, this approach is the most direct and objective for consistency amongst a family of materials examined in the same way. The onset of the melting peak is also used and represents a lower bound on the true melting point, but is subject to a degree of researcher subjectivity because of the need to estimate both the baseline and the leading-edge tangent of the peak. The onset of the peak is also disrupted strongly by impurities in the sample. In this work we report both onset and peak and refer to the former throughout the paper as it is likely to be closer to (though below) the true value.

Extended thermal cycling

Extended thermal cycling was conducted on a Perkin Elmer DSC 8000 at a ramp rate of 10 °C/min. Samples were cycled between temperatures ~ 40 °C below and 10 °C above their respective melting points. The consistency of T_m and ΔH_f was used to indicate stability. Representative thermal cycling data is shown in Figure S15.

Single-crystal X-ray crystallography

Data was collected at 100 K on the Micro Crystallography – MX2 beamline at the Australian Synchrotron.[1] The data collection and integration were performed within the Blu-Ice[2] and XDS software programs.[3] The structures were solved and refined using the SHELX[4,5] software suite, and refined against F^2 using Olex2[6] as a graphical interface. Alkyl hydrogen atoms were placed in calculated positions using the riding model, and the urethane N-H protons were modelled based on electron density, with restrained N-H bond lengths of 0.91(2) using the DFIX restraint. Due to hardware constraints, including a phi axis rotation only and a minimum available detector distance, the data is limited resulting in a low completeness (approximately 92%). However, the overall data to parameter ratio is greater than 10.

Notably, obtaining crystals with suitable diffraction for structure refinement was very challenging, and upwards of 25 crystals were mounted for each sample before suitable diffraction was achieved. The successful crystals were obtained by slow-cooling samples of C18-hx and C18-MDP from the melt.

Table S1. Crystal data and structure refinement details for C18-hx and C18-MDP

Identification code	**C18-hx**	**C18-MDP**
CCDC identifier	2220003	2220004
Empirical formula	$C_{44}H_{88}N_2O_4$	$C_{51}H_{86}N_2O_4$
Formula weight/g.mol^{-1}	709.16	791.21
Temperature/K	100.15	100(2)
Crystal system	triclinic	monoclinic
Space group	P-1	$P2_1/m$
a/Å	4.9030(10)	5.0770(10)
b/Å	5.4300(11)	93.923(19)
c/Å	43.425(9)	5.4320(11)
α/°	88.35(3)	90
β/°	92.03(3)	115.03(3)
γ/°	71.30(3)	90
Volume/Å^3	1093.4(4)	2347.0(10)
Z	1	2
***p* calc/g/cm^3**	1.077	1.120
μ/mm^{-1}	0.067	0.069
F(000)	398.0	876.0
Crystal size/mm^3	0.055 × 0.035 × 0.025	0.12 × 0.06 × 0.03
Radiation	synchrotron (λ = 0.710923)	synchrotron (λ = 0.710764)
2Θ range for data collection/°	1.878 to 64.566	0.868 to 51.988
Index ranges	-6 ≤ h ≤ 6, -7 ≤ k ≤ 7, -63 ≤ l ≤ 63	-6 ≤ h ≤ 6, -115 ≤ k ≤ 115, -6 ≤ l ≤ 6
Reflections collected	18816	28231
Independent reflections	5613 [R_{int} = 0.0734, R_{sigma} = 0.0692]	4285 [R_{int} = 0.1791, R_{sigma} = 0.1170]
Data/restraints/parameters	5613/1/231	4285/0/299
Goodness-of-fit on F2	0.945	1.063
Final R indexes [I>=2σ (I)]	R_1 = 0.0888, wR_2 = 0.2505	R_1 = 0.1254, wR_2 = 0.3363
Final R indexes [all data]	R_1 = 0.1182, wR_2 = 0.2807	R_1 = 0.1473, wR_2 = 0.3481
Largest diff. peak/hole / e Å^{-3}	0.31/-0.27	0.33/-0.26

Table S2. Distances and angles of hydrogen bonds in C18-hx and C18-MDP

Compound	**Donor**	**Proton**	**Acceptor**	**D-H (Å)**	**H···A (Å)**	**D···A (Å)**	**D-H···A(°)**
C18-hx	N1	H1	O2	0.899(15)	1.983(15)	2.880(2)	175.1(19)
C18-MDP	N1	H1	O1	0.84(2)	2.10(4)	2.909(4)	161(3)

Powder X-ray diffraction

Powder X-ray diffraction patterns were collected at ambient temperature on a Bruker D8 Advance equipped with Cu-Kα radiation (λ = 1.54 Å). A step time of 0.1 s was used with a step size of 0.021°.

Accelerated rate calorimetry (ARC)

The Accelerated Rate Calorimetry instrument records self-heat rate as a function of temperature while also giving time vs temperature and temperature vs pressure profiles. Experiments were carried out with identical sample masses to reduce variation on thermal inertia between samples. Between 0.5 g and 1 g of samples were loaded into the titanium ARC sample bomb equipped with thermocouples and a pressure transducer in a closed environment as per the figure below. The samples were then subjected to heat-wait-search mode with outputs recorded. Samples were repeated twice to ensure consistency of data, and experiments were carried out in both N_2 and air atmospheres.

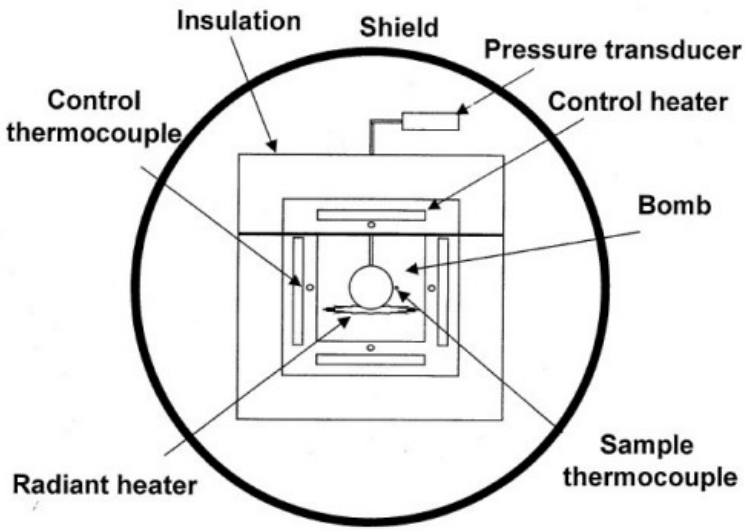

Figure S1. Accelerating rate calorimeter. Figure from[7].

A thermal inertia (ϕ) correction compensates for heat loss to the sample container during the experiment using the following formula (ASTM E1981):

$$\Phi = \frac{(m_s + C_{p,s} + m_c + C_{p,c})}{m_s C_{p,s}}$$

where m_s = the mass of the sample, m_c = the mass of the container, $C_{p,c}$ = the heat capacity of the container and $C_{p,s}$ = the heat capacity of the sample.

Nuclear Magnetic Resonance Spectroscopy (NMR)

Solution-state ^{1}H NMR spectra were recorded at in either $CDCl_3$ or d_8-THF at 298 K on a Bruker Avance III NMR spectrometer equipped with a 9.4 T magnet and 5 mm TBO probe, operating at 400.13 MHz. Chemical shifts (δ) are reported in parts per million (ppm) and were referenced to the residual d_8-THF or $CDCl_3$ solvent signals. As a result of poor solubility, only ^{1}H NMR spectra were able to be collected on each of the materials.

Infrared spectroscopy

An arbitrarily thin layer of the samples was deposited onto a mirror finished (#8) grade 304 stainless steel slide by dissolving the compound in THF, dropping the solution on the slide and allowing the THF to evaporate. The slide was transferred to a Linkam FTIR600 sample stage and analysed in a transflection geometry using an Agilent Cary 670 FTIR spectrometer coupled to an Agilent Cary 620 IR microscope with a 15x objective. Spectra were recorded in the region between 4000^{-1} and 600 cm^{-1} at a resolution of 4 cm^{-1} using the microscopes LN2 cooled Mercury Cadmium Telluride (MCT) detector. 64 scans were recorded for the background and sample acquisition. The background was recorded on a clean region of the slide prior to analysis. The sample was left to equilibrate at each temperature for 60 seconds before spectra acquisition.

Spectra were preprocessed by calculating the 2nd derivative spectra using the Savitsky-Golay method (window size of 19, 2nd order polynomial) and subsequently normalised over the whole spectral region. Preprocessing was performed using Quasar.[8]

Mass spectrometry

Analysis was carried out at the School of Chemistry, Monash University. A 10 µL injection volume of test compound was used in conjunction with a 3 minute isocratic gradient of acetonitrile with 0.1% formic acid over a 3 minute run time an Agilent 1200 series LC (Santa Clara, CA, USA). Analysis was conducted on a Agilent 6450 QTOF MS system (Santa Clara, CA, USA) with a dual ESI source. The MS was operated in positive or negative mode using the following conditions: nebulizer pressure 45 psi, drying gas flow-rate 10 L/min, gas temperature 300°C, capillary voltage 4000/-4000 V, fragmentor 170 V and skimmer 65 V. The instrument was operated in the extended dynamic range mode with data collected in m/z range 100–1500.

Thermogravimetric analysis

Thermogravimetric analysis experiments were conducted using a Mettler Toledo TGA/DSC 1 STARe system. Samples were between 5 mg and 20 mg and contained in hermetically sealed aluminium pans. Samples were either heated at a dynamic heating rate of 10 K/min over the temperature range 298 K – 823 K, or held at specified temperatures for the isothermal experiments. In both cases a nitrogen flow of 20 mL/min was used.

Flash point analysis

Flash point analysis of C18-hx was conducted by Sharp and Howells Pty Ltd, using a SYD-3536 Cleveland Open-Cup Flash Point tester. Approximately 105 g of material was used for the analysis. A flash point was detected between 280 °C – 290 °C.

3. Calculations

Cost analysis

Prices of starting materials were found on Alibaba, in November 2022 and are shown in Table S2.

Table S3. Prices of raw materials for the synthesis of C18-hx and C18-MDP

Material	CAS	Price	Reference
1,6-hexamethylene diisocyanate	822-06-0	$0.3 USD/kg	[9]
4,4'-methylenebis(phenyl isocyanate)	101-68-8	$1 USD/kg	[10]
Octadecanol	112-92-5	$500 USD/tonne	[11]

Table S4. Calculations for total prices per tonne of PCM for C18-hx and C18-MDP

	C18-hx	C18-MDP
ΔH_f	200	147
kWh/tonne	57	41
Molar mass	709.1 g mol^{-1}	791.26 g mol^{-1}
Diisocyanate used in synthesis	1,6-hexamethylene diisocyanate	4,4'-methylenebis(phenyl isocyanate)
Diisocyanate molar mass	168.19 g mol^{-1}	250.25 g mol^{-1}
Stearyl alcohol molar mass	270.49 g mol^{-1}	270.49 g mol^{-1}
Mass ratio diisocyanate:stearyl alcohol	1:3.22	1:2.16
Mass diisocyanate/tonne PCM	237 kg	316 kg
Mass stearyl alcohol/tonne PCM	763 kg	684 kg
Cost diisocyanate/tonne PCM	$71.1 USD	$316 USD
Cost stearyl alcohol/tonne PCM	$381.5 USD	$342 USD
Cost of PCM	$453 USD/tonne	$658 USD/tonne
Cost / kWh for 1 cycle	$7.9 USD/kWh	$8.3 USD/kWh
Cost / kWh over 5 years (1825 cycles)	$0.0043 USD/kWh	$0.0046 USD/kWh

CO_2 equivalents calculations

C18-hx

Energy stored: ΔH_f = 200 J/g, = 57 kWh/tonne

CO_2 emissions/kg from use of 1,6-hexamethylenediisocyanate

6500 kg CO_2/tonne * 0.237 tonne = 1541 kg CO_2/tonne PCM

therefore 27 kg CO_2/kWh

assuming 5 year lifetime, 365 days * 5 = 1825 cycles

0.0015 kg CO_2/kWh

C18-MDP

Energy stored: ΔH_f = 147 J/g, = 41 kWh/tonne

CO_2 emissions/kg from use of 4,4'-methylenebis(phenyl isocyanate)

2760 kg CO_2/tonne * 0.316 tonne = 872 kg CO_2/tonne PCM

therefore 21.3 kg CO_2/kWh

assuming 5 year lifetime, 365 days * 5 = 1825 cycles

21.3 kg / 1825 cycles = 0.0011 kg CO_2/kWh

4. Supplemental figures

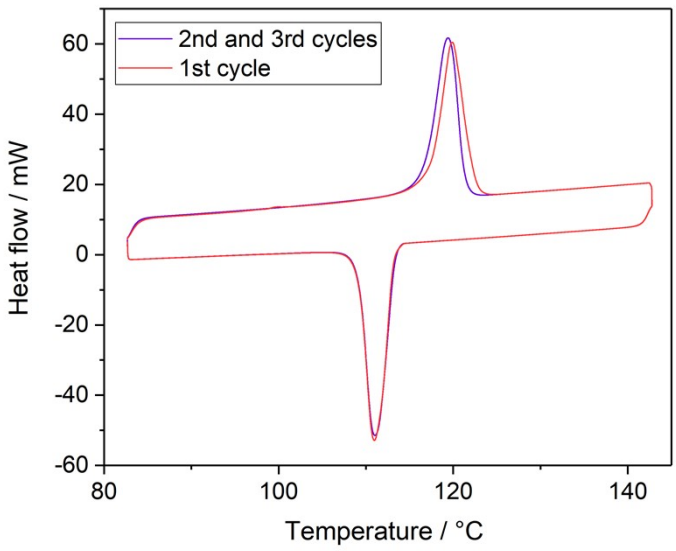

Figure S2. DSC curve of C18-hx with a ramp rate of 10 °C/min.

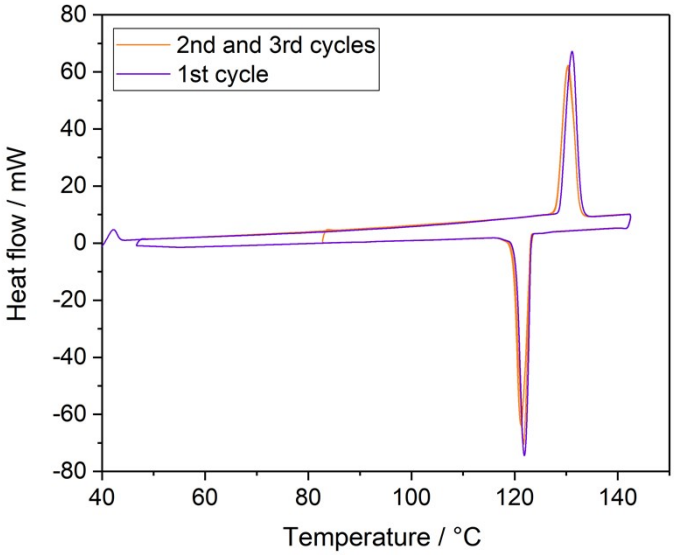

Figure S3. DSC curve of C18-MDP with a ramp rate of 10 °C/min.

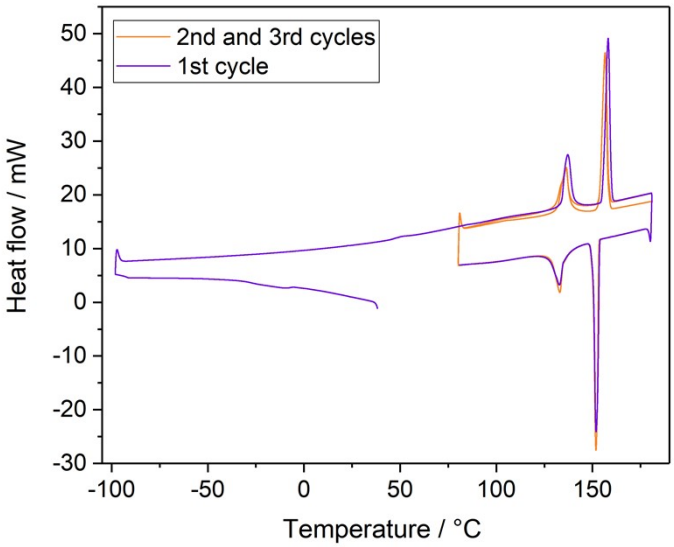

Figure S4. DSC curve of C18-cyhx with a ramp rate of 10 °C/min.

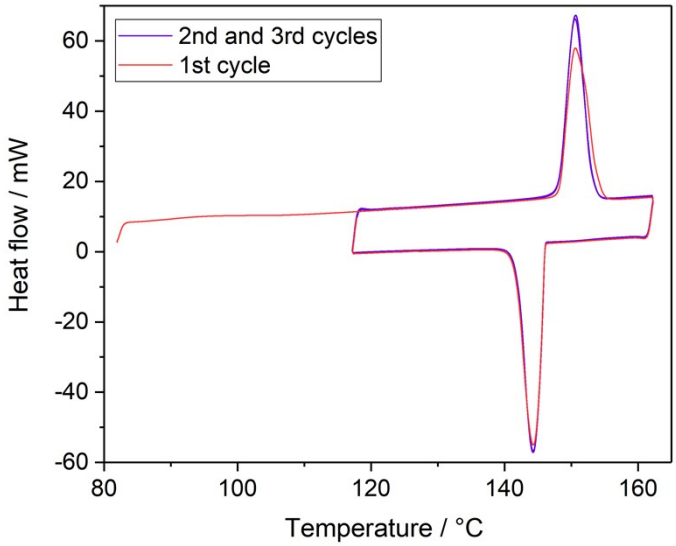

Figure S5. DSC curve of C18-Ph with a ramp rate of 10 °C/min.

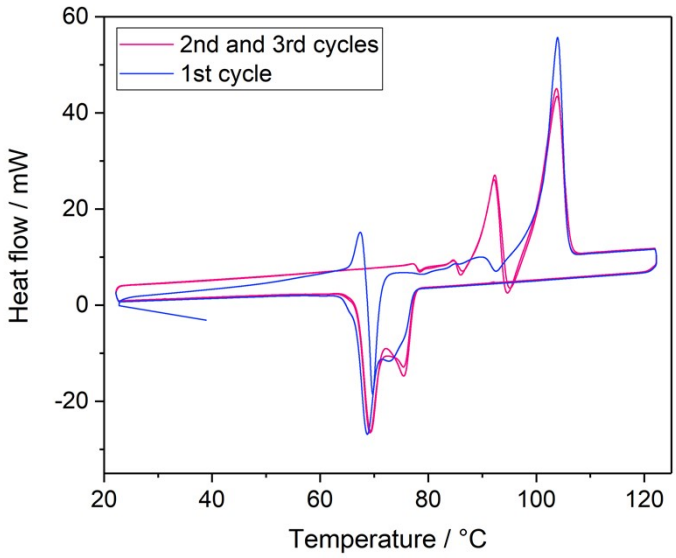

Figure S6. DSC curve of C18-MePh with a ramp rate of 10 °C/min.

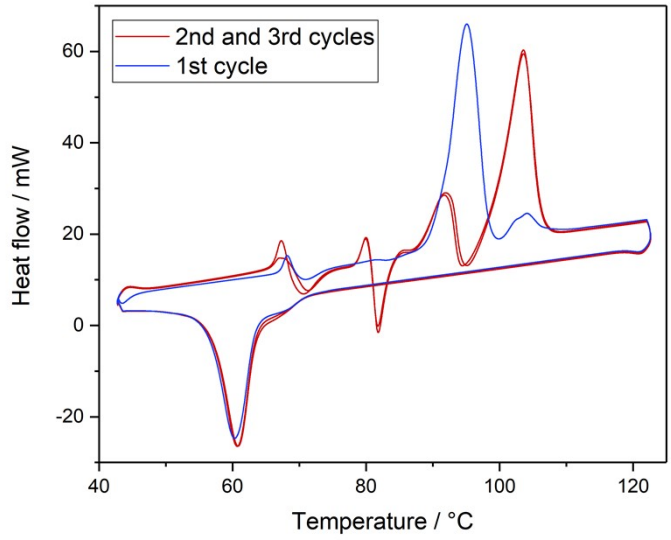

Figure S7. DSC curve of C18-MePh with a ramp rate of 20 °C/min.

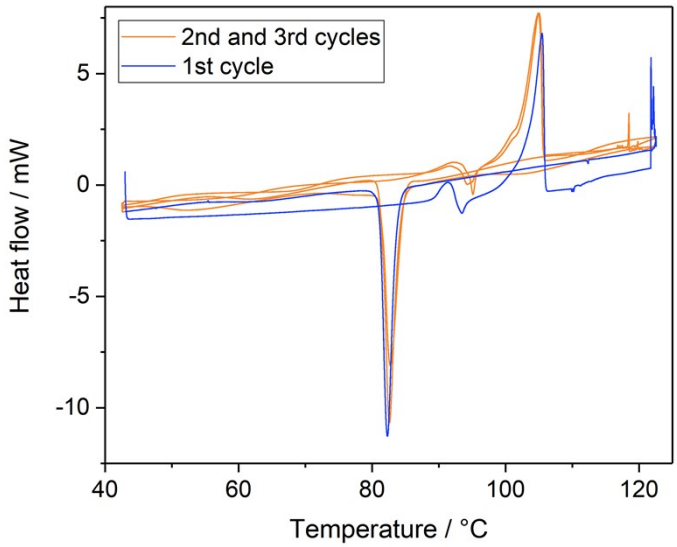

Figure S8. DSC curve of C18-MePh with a ramp rate of 1 °C/min.

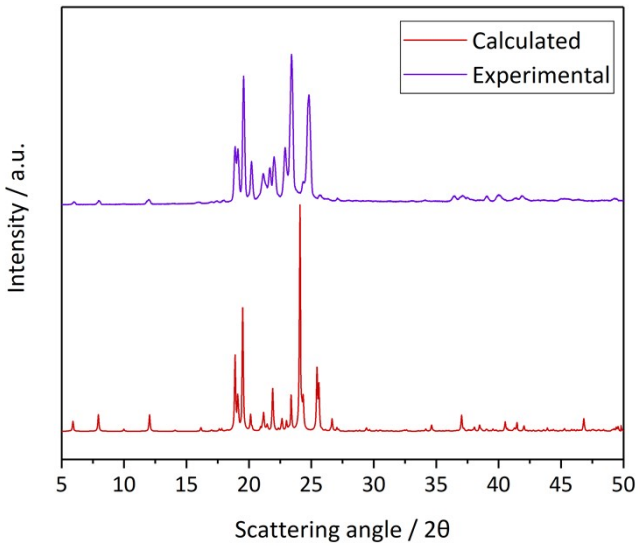

Figure S9. Experimental powder pattern of C18-MDP (purple) and PXRD pattern of C18-MDP calculated from the single-crystal structure.

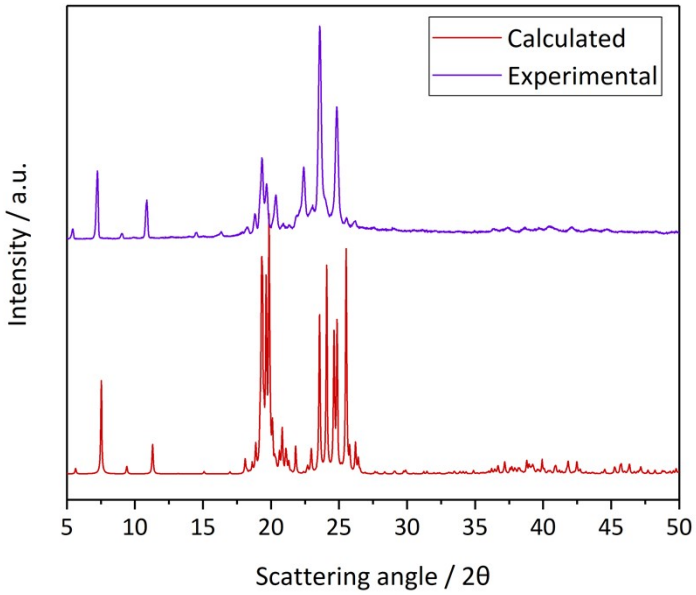

Figure S10. Experimental powder pattern of C18-MDP (purple) and PXRD pattern of C18-hx calculated from the single-crystal structure.

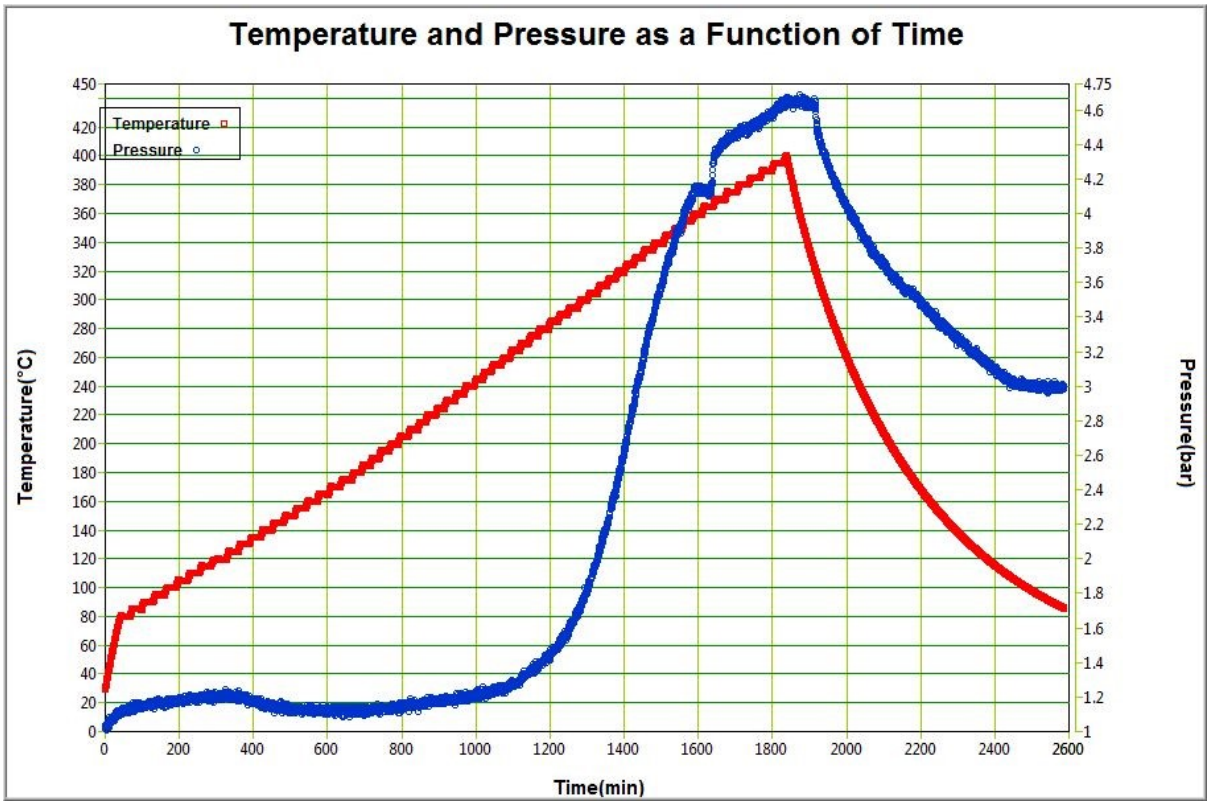

Figure S11. ARC results showing temperature and pressure as a function of time for C18-hx under an air atmosphere.

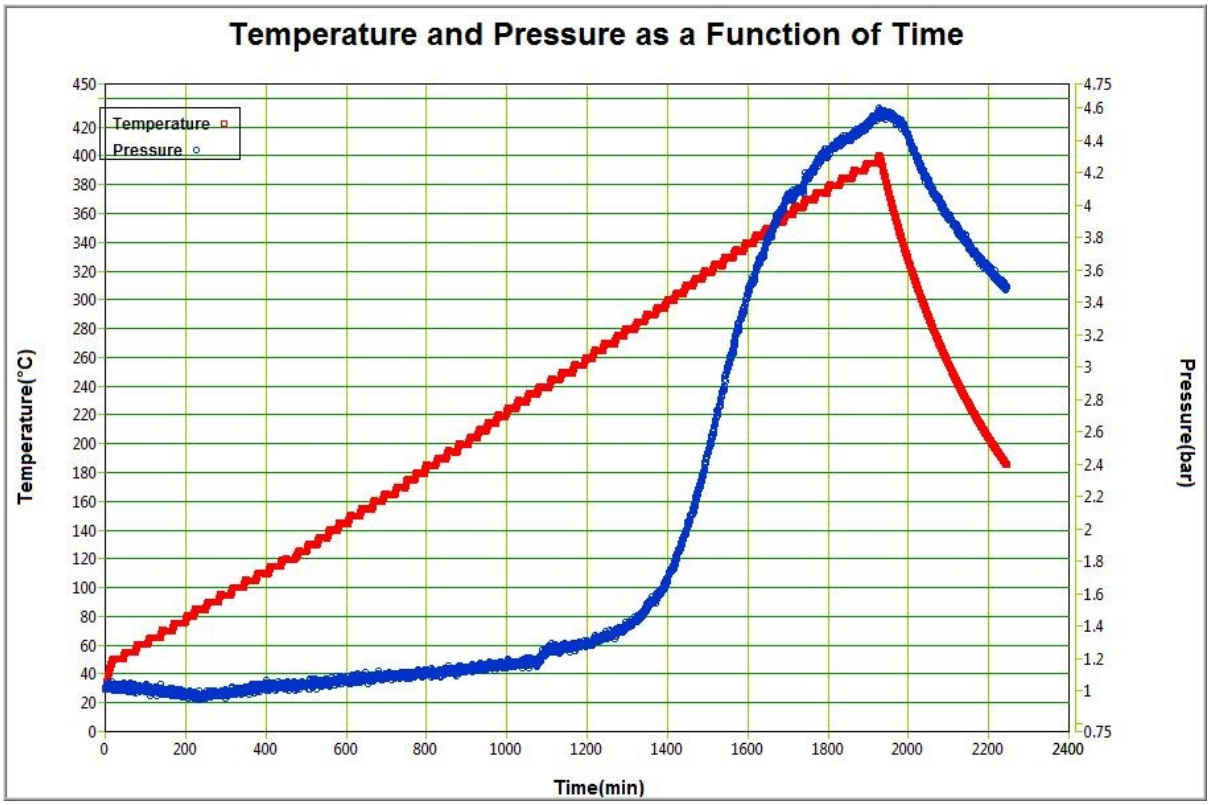

Figure S12. ARC results showing temperature and pressure as a function of time for C18-hx under a nitrogen atmosphere.

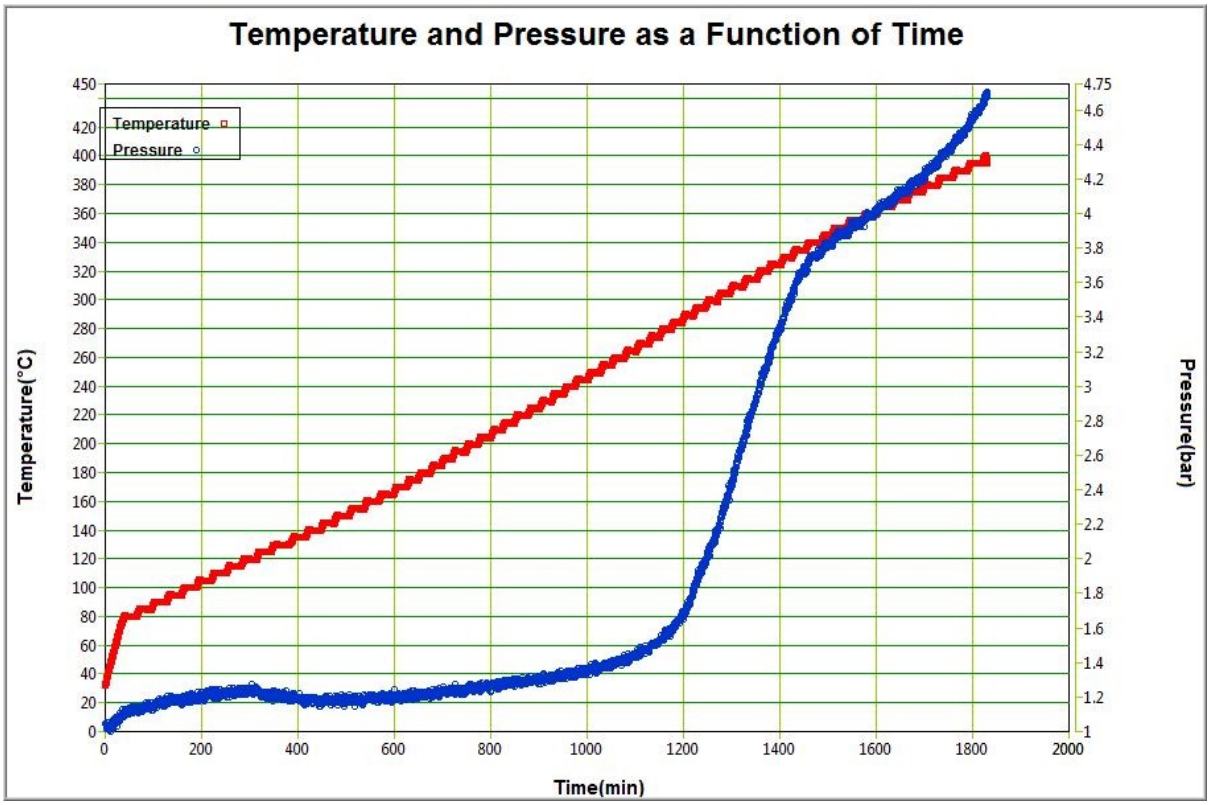

Figure S13. ARC results showing temperature and pressure as a function of time for C18-MDP under an air atmosphere.

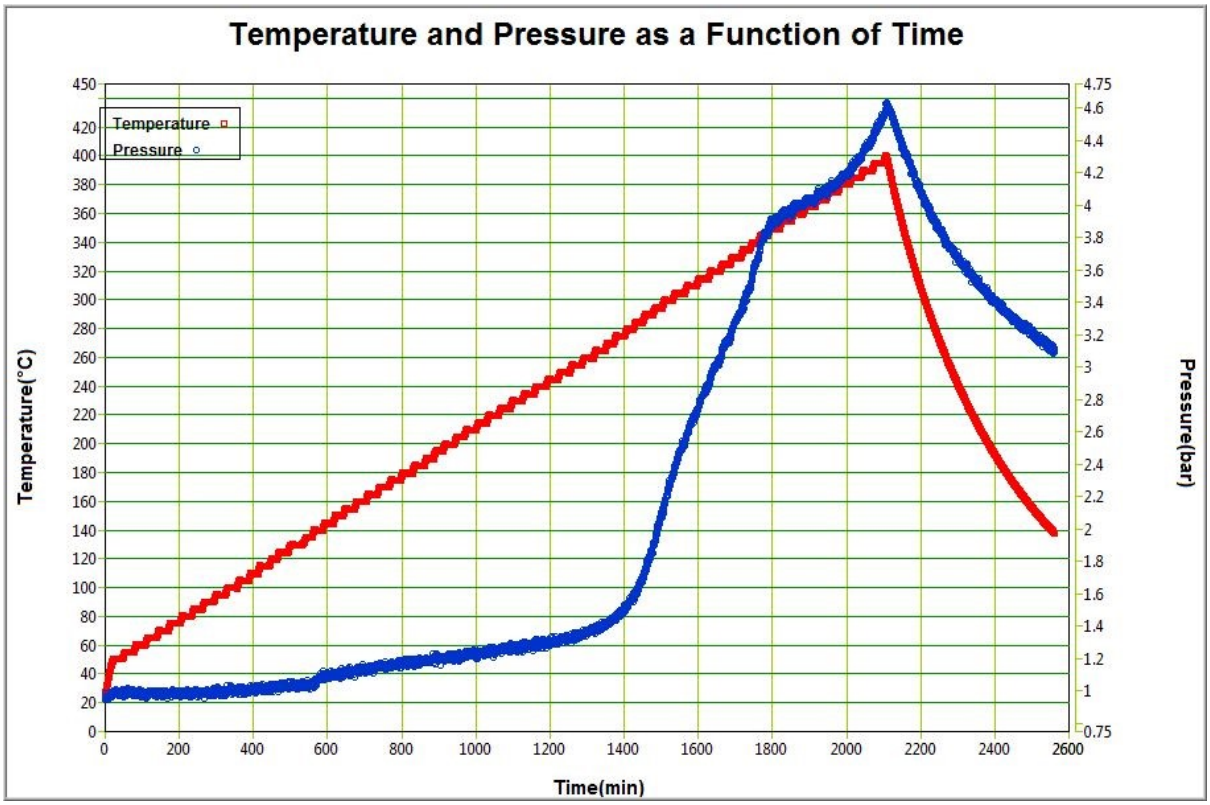

Figure S14. ARC results showing temperature and pressure as a function of time for C18-MDP under a nitrogen atmosphere.

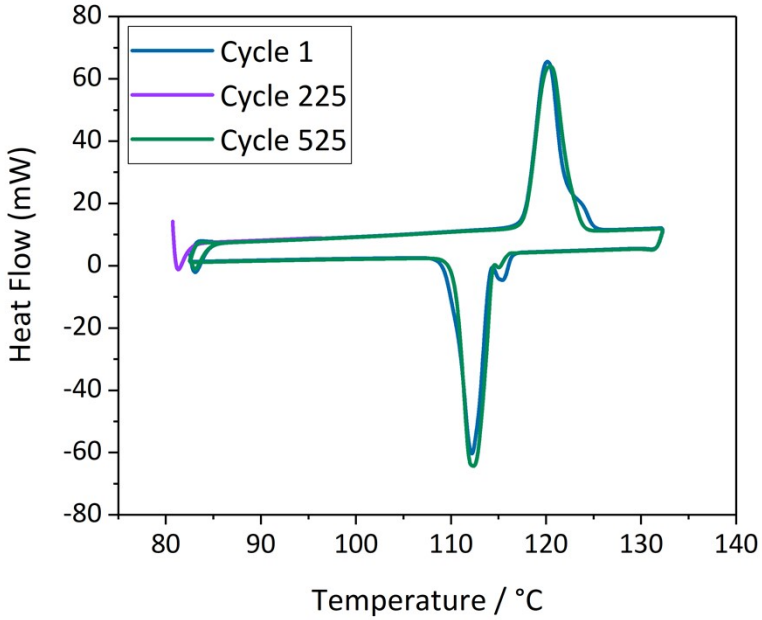

Figure S15. Representative thermal cycling data showing the DSC curves of C18-hx after various numbers of heating and cooling cycles.

5. References

1 D. Aragão, J. Aishima, H. Cherukuvada, R. Clarken, M. Clift, N. P. Cowieson, D. J. Ericsson, C. L. Gee, S. Macedo and N. Mudie, *J. Synchrotron Radiat.*, 2018, **25**, 885–891.

2 T. M. McPhillips, S. E. McPhillips, H.-J. Chiu, A. E. Cohen, A. M. Deacon, P. J. Ellis, E. Garman, A. Gonzalez, N. K. Sauter and R. P. Phizackerley, *J. Synchrotron Radiat.*, 2002, **9**, 401–406.

3 W. Kabsch, *J. Appl. Crystallogr.*, 1993, **26**, 795–800.

4 G. M. Sheldrick, *Acta Crystallogr. Sect. C Struct. Chem.*, 2015, **71**, 3–8.

5 G. M. Sheldrick, *Acta Crystallogr. Sect. Found. Adv.*, 2015, **71**, 3–8.

6 O. V. Dolomanov, L. J. Bourhis, R. J. Gildea, J. A. Howard and H. Puschmann, *J. Appl. Crystallogr.*, 2009, **42**, 339–341.

7 M. Surianarayanan, R. Vijayaraghavan, G. Swaminathan and P. Rao, *Curr. Sci.*, 2001, **80**, 738–747.

8 M. Toplak, S. T. Read, C. Sandt and F. Borondics, *Cells*, 2021, **10**, 2300.

9 Hexamethylene Diisocyanate Cas 822-06-0 - Buy Hexamethylene Diisocyanate,Desmodurn,1 6-diisocyanato-hexan Product on Alibaba.com, https://www.alibaba.com/product-detail/hexamethylene-diisocyanate-CAS-822-06-0_1600514802595.html?spm=a2700.galleryofferlist.normal_offer.d_image.622e3b5c7he9uK, (accessed November 22, 2022).

10 Adequate Supply Methylene Diphenyl Diisocyanate Cas 101-68-8 - Buy Buy Methylene Diphenyl Diisocyanate,Cas 101-68-8,Methylene Diphenyl Diisocyanate Cas 101-68-8 Product on Alibaba.com, https://www.alibaba.com/product-detail/Adequate-supply-Methylene-diphenyl-diisocyanate-CAS_1600546713054.html?spm=a2700.galleryofferlist.normal_offer.d_image.4781c97aMGqMOA, (accessed November 22, 2022).

11 China Factory Supply Octadecanol Cas 112-92-5 1-octadecanol Stearyl Alcohol For Surfactant - Buy Best Price Octadecanol,1-octadecanol,High Quality Stearyl Alcohol Product on Alibaba.com, https://www.alibaba.com/product-detail/China-Factory-Supply-Octadecanol-CAS-112_1600596440060.html?spm=a2700.galleryofferlist.normal_offer.d_image.5f7765f3RqB84i, (accessed November 22, 2022).